Intervalence-band THz laser in selectively-doped semiconductor structure

M. V. Dolguikh, A.V. Muravjov, R. E. Peale
Dept. of Physics, University of Central Florida, Orlando FL, 32816-2385

ABSTRACT

Monte Carlo simulation of carrier dynamics and far-infrared absorption in a selectively-doped p-type multi-layer Ge structure with vertical transport was performed to test a novel terahertz laser concept. The design exploits the known mechanism of THz amplification on intersubband transitions in p-Ge, but with spatial separation of light hole accumulation regions from doped regions, which allows remarkable enhancement of the gain. The structure consists of doped layers separated by 300-500 nm gaps of pure-Ge. Vertical electric field (~ 1-2 kV/cm) and perpendicular magnetic field (~ 1T) provide inversion population on direct intersubband light- to heavy-hole transitions. Heavy holes are found to transit the undoped layers quickly and to congregate mainly around the doped layers. Light holes, due to tighter magnetic confinement, are preferably accumulated within the undoped layers. There the relatively small ionized impurity and electron-electron scattering rates allow higher total carrier concentrations, and therefore higher gain, than in bulk crystal p-Ge lasers. In contrast to GaAs-based THz quantum cascade lasers (QCL), the robust design and large structure period suggest that the proposed Ge structures might be grown by the chemical vapor deposition (CVD) method. The ability of CVD to grow relatively thick structures will simplify the electrodynamic cavity design and reduce electrodynamic losses in future THz lasers based on the presented scheme.

INTRODUCTION

Recent semiconductor-laser developments in the terahertz range of the electromagnetic spectrum include intervalence band p-Ge lasers [1], Si lasers based on optically pumped donors [2], and quantum cascade lasers (QCL) [3-5]. A fundamental challenge for any THz solid-state laser is intrinsic far-IR absorption by lattice vibrations, which increases rapidly with temperature. Operation of solid-state far-infrared lasers at elevated temperatures can be achieved only if the gain is sufficiently high. This requires high carrier density, but ionized impurity scattering and electron-electron interaction increase with density and generally work against the conditions needed for high gain. Improvements in QCL technology in overcoming these problems have been very rapid recently, with continuous wave output and operation temperatures above liquid nitrogen reported. However, because of high growth accuracy requirements, QCLs can be grown by technologically advanced molecular beam epitaxy method (MBE) only, which limits maximal structure thickness. To obtain high laser Q at the long THz wavelengths, structures should ideally be more than 10 micrometers thick.

In bulk crystal p-Ge lasers, population inversion grows for certain ratios of electric and magnetic fields when light holes are accumulated on closed trajectories below the optical phonon energy, while heavy holes undergo rapid optical phonon scattering. Averaged over the ensemble of particles, cyclotron orbits in crossed E and B fields have different average radii for different effective mass. Light holes, drifting in the $\vec{E} \times \vec{B}$ direction, are free from optical phonon scattering and their 10-100 ps life time is defined only by scattering on acoustic phonons and impurity centers. Heavy holes have larger orbits and gain sufficient kinetic energy from the electric field to reach the optical phonon scattering threshold. Thus, their lifetime is only ~ 1 ps. This allows generation of an inversion population and the possibility of amplification on direct optical transitions between light and heavy hole subbands.

As an alternative to bulk p-Ge lasers, innovative structures composed of doped and undoped regions of p-type semiconductor were studied in this work (Fig. 1). The spatial period of the structure was chosen smaller than the average Larmor radius of heavy hole trajectories in the crossed E and B fields, but larger than the average Larmor radius of light holes. The higher impurity-scattering rate for heavy holes assists in the accumulation of light holes.

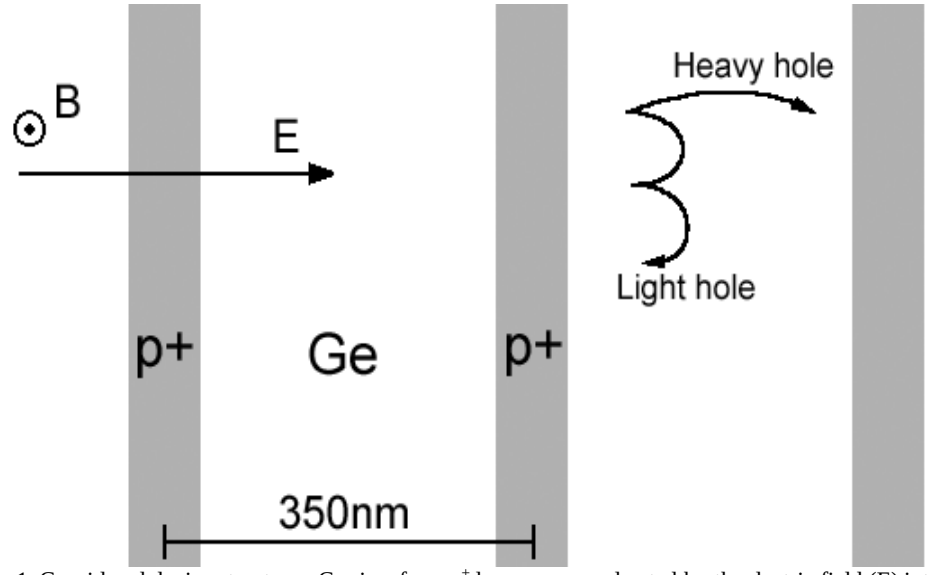

Fig. 1. Considered device structure. Carriers from p^+ layers are accelerated by the electric field (E) into cyclotron orbits determined by the perpendicular magnetic field (B). Fields are tuned so that the average light-hole orbits are smaller than the doping period while heavy holes suffer strong impurity scattering at the doped layers.

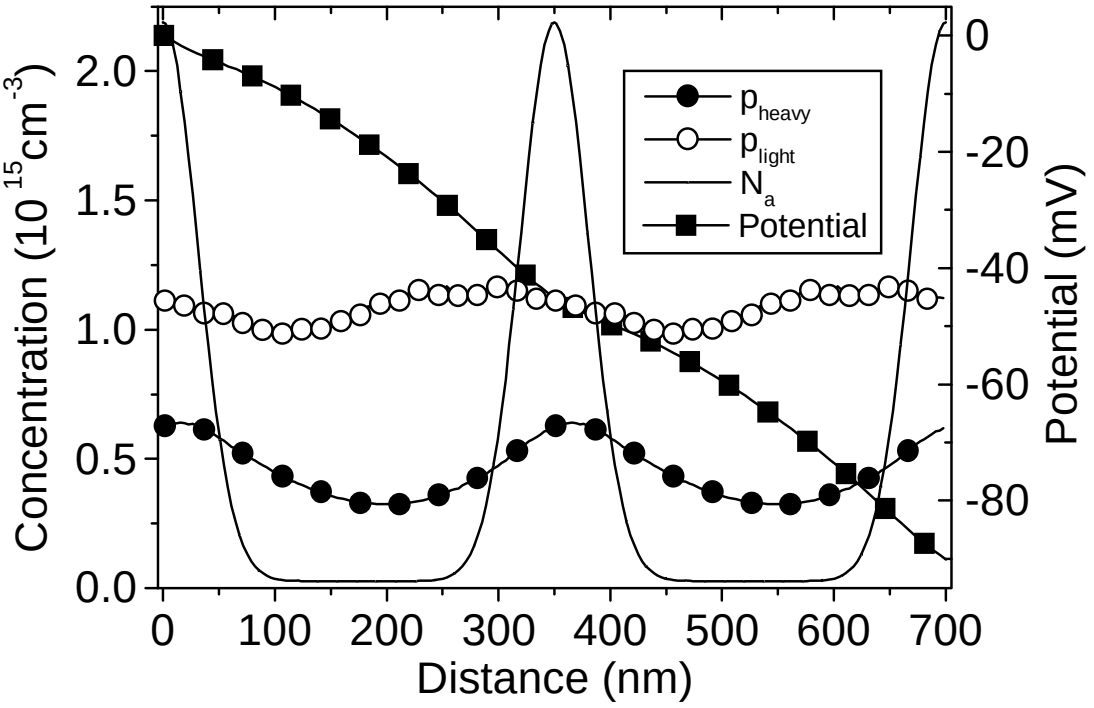

Fig. 2. Equilibrium potential distribution, concentration of light (multiplied by $(\frac{m_h}{m_l})^{\frac{3}{2}}$) and heavy holes and acceptor concentration across the structure for applied fields E=1.25kV/cm, B=1T and $N_{av} = 5*10^{14}\text{cm}^{-3}$.

METHODS

The Monte Carlo computational model simulates free carrier motion in the Ge valence band for crossed electric and magnetic fields and cryogenic temperatures. The effective hole temperature reached by electric field (~ 1kV/cm) heating is 100-200 K, i.e. much higher than the lattice temperature (4 K). This heating is bounded by the optical phonon energy (430 K, 37 meV). The period of the structure considered is ~ 350 nm and the typical magnetic field is ~1T. Energy quantization due to magnetic field and confinement is considered negligible, which permits a classical approach to the hole spectrum and equations of motion.

Carrier dynamics are simulated using classical motion equations and scattering probabilities to numerically solve the Boltzmann equation [6,7]. Time or ensemble averaged momentum and position yield the hole distribution functions $f_{l,h}(\vec{k},\vec{r})$ (subband (l,h), wavevector k and coordinate r). Two valence sub-bands (light and heavy holes) with isotropic and parabolic dispersion laws were considered. The standard Rees rejection technique chooses among scattering processes [6]. The rate of each scattering process is given by an analytic expression. Optical phonon scattering is treated in a deformation potential approximation [8,9]. Acoustic phonon scattering is simplified according to [10]. Inelasticity is included using [11].

The unscreened Ridley formula [12] with Brooks-Herring inter(intra) subband coefficients [11] is used for ionized impurity scattering. Statistically distributed solid angles of hole motion direction were used to calculate electron-electron scattering by a modification of the method that was used for ionized impurity scattering. These features in our MC procedure are new and differ from the approach to ionized impurity and electron-electron scattering that have been employed previously in p-Ge crystal laser simulations (see [13]). Besides being logically preferable, they predict results in better agreement with experiment than previous p-Ge laser MC simulations (see Appendix A).

Monte Carlo code was specially written to include spatially varying scattering probabilities, which permitted simulation of carrier dynamics in media with stratified parameters, e.g. the structure with varying doping profile. Fig. 1 is a schematic of the preliminary structure considered. For simulations presented here, the structure period d was chosen to be 350 nm. Geometry of the structure allows the infinite charged planes approximation (size of the sample in the directions perpendicular to doped layers is very large compared to structure period).

Preliminary calculations indicated that redistribution of space charge influences the carrier dynamics at average concentrations above $10^{14}\,cm^{-3}$ at considered structure periods of 350-400 nm. The redistribution of space charge was included in the form of an additional "internal" electric field. Iteration was used to find self-consistent solution of the Poisson equation and thereof the spatial carrier distribution and potential profile. Total electric field across the structure is given by $E = -\frac{\partial \varphi}{\partial x} = E_{ext} + E_{int}$, where E_{ext} is the applied external field, and φ is electric potential. For any distribution of holes p(x) and negatively charged acceptor impurity centers N(x), the internal electric field along the period of the structure d is given by:

$$E_{int}(x) = \frac{e}{2\varepsilon\varepsilon_0}\left[\int_0^x [p(x) - N(x)]dx - \int_x^d [p(x) - N(x)]dx\right] \quad (1)$$

where ε is the relative dielectric constant, ε_0 is the permittivity of free space, and e is the electron charge. Due to total neutrality of the crystal $E_{int}(0) = E_{int}(d) = 0$.

Small signal gain is calculated from the negative absorption of radiation due to direct inter subband (light to heavy) transitions and free carrier absorption assisted by phonons or ionized impurities [11]. In this case the absorption cross-section is proportional the integral over k of the difference $z_{lh}(k)[f_h(k,r) - f_l(k,r)]d(e_l(k) - e_h(k) - h\nu)$, where the distribution functions $f_{l,h}(\vec{k},\vec{r})$ for light and heavy holes are simulation outputs, $e_{l,h}(k)$ are hole energies, and $z_{lh}(k)$ is the unpolarized oscillator strength [14]. The total absorption cross section due to indirect transitions is given by the integral over the total indirect transition probability from an initial state (n,k,r) to all possible final states (n',k',r) due to absorption or emission of a photon, assisted by scattering.

RESULTS

Each period of the considered structure consisted of 0.8d pure germanium ($2.6*10^{13}$ cm^{-3} acceptor concentration) and 0.2d doped at concentrations $3.5*10^{14}$ - $5*10^{15}$ cm^{-3}. This results in an average hole and acceptor concentration $N_{av} = 9*10^{13}$ - $1*10^{15}$ cm^{-3} (zero compensation is assumed). Doping profiles have been chosen in the form of the solution to the diffusion equation [15], simulating possible acceptor diffusion under high temperature conditions of CVD growth with possible values T=750C and 15min duration (see Fig. 2).

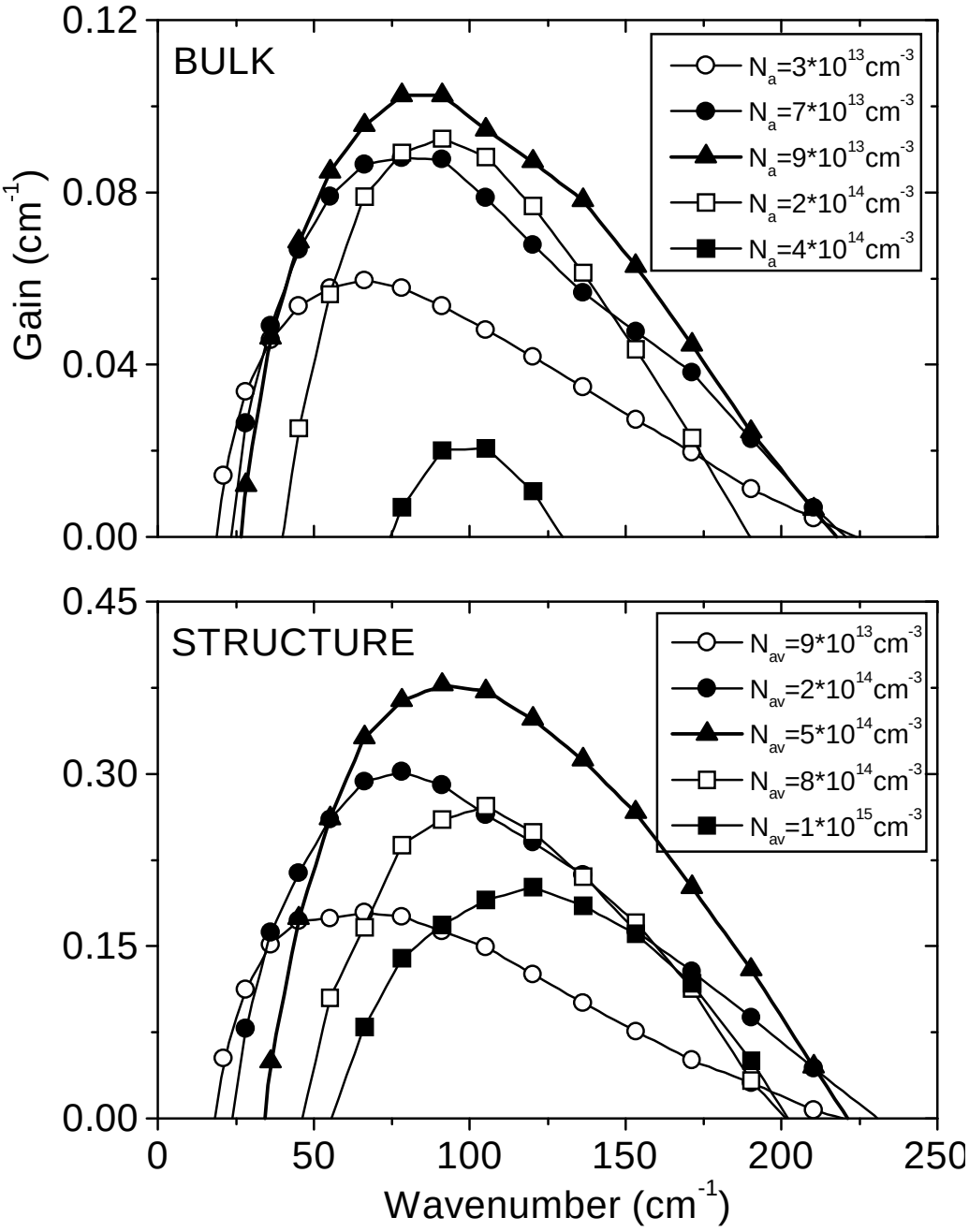

Fig. 3. Bulk crystal and selectively doped structure gain spectra for different acceptor concentration and zero compensation.

The spatial distribution of holes was investigated to determine the space charge and "internal" electric field distribution within the structure due to the static distribution of negative ionized impurity centers and the dynamic distribution of positive holes. For these particular simulations we assumed zero compensation, so that all introduced doping centers are shallow acceptors. Applied external fields are E = 1.25 kV/cm, B = 1T, and the sample temperature is 10K. By introducing appropriate initial p(x), this self-relaxation method converges to a stable distribution of holes p(x) with fixed acceptor distribution N(x). The internal field due to polarization of mobile holes and fixed acceptors is found to be comparable to the external one. The resulting total potential for $N_{av} = 5*10^{14}\ cm^{-3}$ is plotted in Fig. 2 as solid square symbols. The electric field is diminished in the first half of the structure period and augmented in the second (x>170nm). There is no potential well observed at this concentration. Light and heavy hole distributions are also plotted in Fig. 2. The light hole distribution is normalized using the relative density of states for light and heavy subbands (i. e. multiplied by $(\frac{m_h}{m_l})^{\frac{3}{2}}$). The majority of holes are concentrated near the doped layers and most of them are heavy. At the same time, the distribution of light holes has a maximum near the central region of the structure period, which creates strong inversion population there.

Fig. 3 compares spatially averaged gain spectra for bulk p-Ge crystal and the structure from Monte Carlo simulations with different acceptor concentrations and zero compensation. The doping level that gives highest gain in the bulk crystal is $9*10^{13} cm^{-3}$ (in close agreement with experiments [1]). The average acceptor concentration that gives highest gain in the structure is $5*10^{14}\ cm^{-3}$ which exceeds the bulk value by more than a factor 5.

Fig. 4 compares the spatially averaged gain at $100\,cm^{-1}$ for the considered structure for different average acceptor concentrations from Fig. 3, compared with similar results for bulk p-Ge crystal. As noted, the peak concentration value for the structure is more than 5x larger than found for bulk p-Ge crystal for the same conditions. The optical gain goes to zero quickly at concentrations above $10^{15} cm^{-3}$. The optical gain maximum in the range 80-$100\,cm^{-1}$ for the structure is 4 times higher than the value for bulk p-Ge crystal.

The spectral-spatial Far-IR gain distribution is shown in Fig. 5. All negative gain points are truncated at zero level. Positive gain occurs in the spectral region 50-$200\,cm^{-1}$ with local maximum in the central region of the structure period between doped layers. Average gain over the structure is positive.

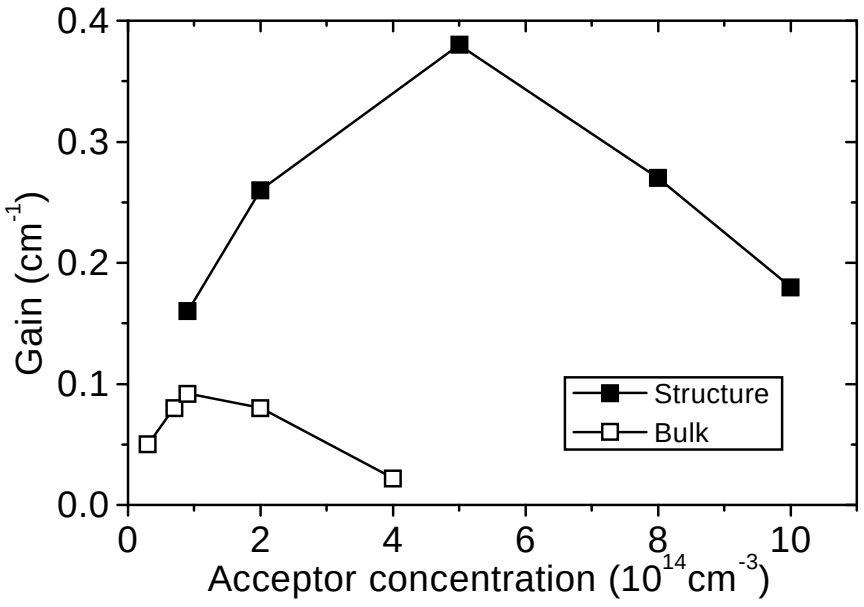

Fig. 4. Gain at 100 cm^{-1} vs. average hole concentration for selectively doped structure and bulk crystal for zero compensation at E=1.25kV/cm, B=1T.

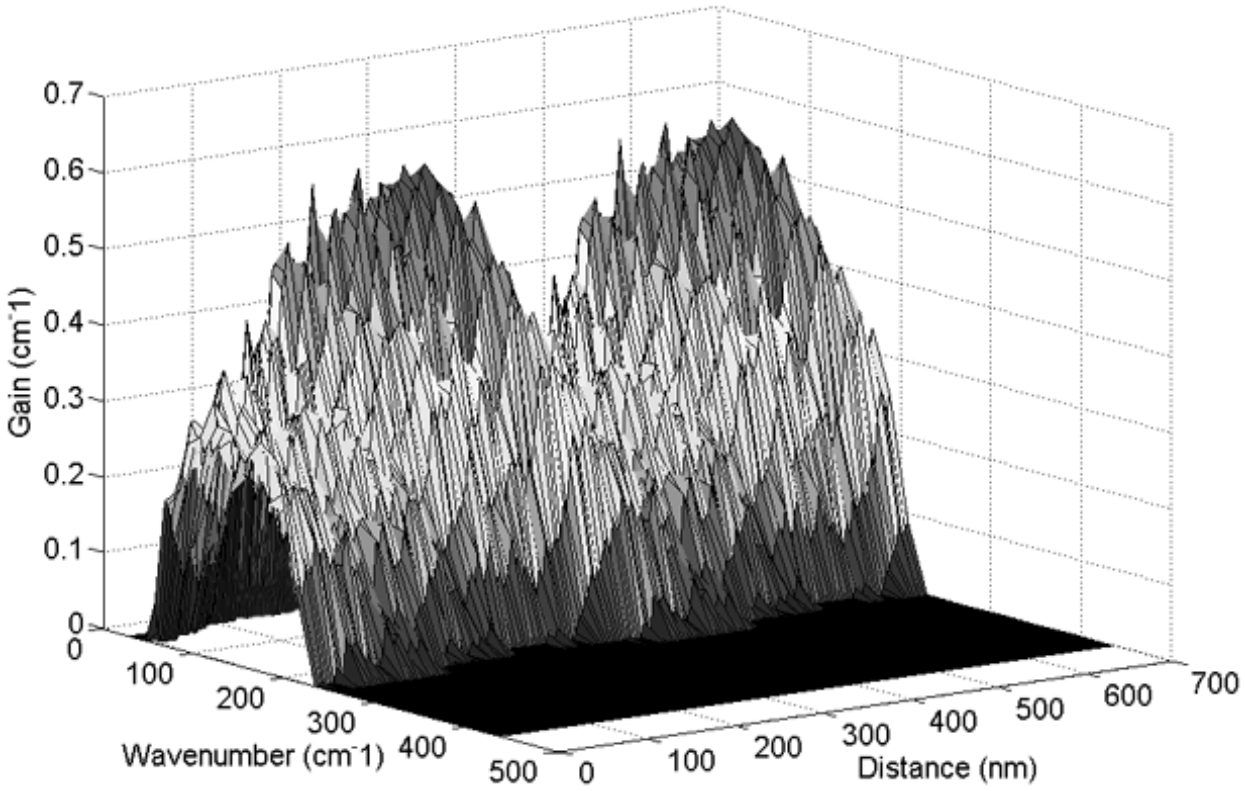

Fig. 5. Gain spectrum distribution across two periods of the structure for E=1.25kV/cm, B=1T and average hole concentration $N_{av} = 5*10^{14} cm^{-3}$.

DISCUSSION AND CONCLUSION

The performed calculations show that THz gain on intersubband hole transitions in crossed electric and magnetic fields in the considered periodically doped Ge structure starts to decrease at remarkably higher average doping concentrations than that for bulk crystal p-Ge laser. Thus, such a structure can provide ~ 4 times higher spatially averaged gain than bulk crystal. Spatial separation of light hole accumulation regions from doped regions makes this possible.

The calculations have been performed at T=10K for a structure consisting of ~ 70nm wide doped layers separated by ~ 280nm wide pure Ge gaps, so that the period of structure is 350nm. Applied electric and magnetic fields are 1.25 kV/cm and 1T, respectively. The maximum calculated local gain is $\sim 0.6\,cm^{-1}$, and the average gain is $\sim 0.4\,cm^{-1}$, while for comparison maximum calculated gain in bulk p-Ge crystal is $\sim 0.1\,cm^{-1}$.

Higher gain in selectively doped Ge structures permits smaller active volume and provides a planar realization of p-Ge laser, which facilitates heat extraction. At the same time, higher gain allows lower electric field threshold, and hence lower Joule heating. This will lead to higher duty cycle and perhaps to CW operation.

The simplicity of proposed structure and potential use of the CVD growth method permit structures of remarkable thickness compared to existing QCL structures grown by MBE. Also note, that in comparison with QCL, the considered Ge structure has a very broad gain spectrum of $50-200 cm^{-1}$, so that stimulated THz emission can be tuned within this region by means of intracavity frequency selection.

APPENDIX A

This appendix collects results for bulk crystal p-Ge laser obtained using the Monte Carlo simulation code we developed. The new thing for this MC code over previous authors is that a more logical impurity scattering and electron-electron scattering procedure was implemented. The code includes a modified ionized impurity scattering and electron-electron interaction model, which, on our opinion, more adequately describes hot hole dynamics under the conditions of the p-Ge laser. These modifications were made in order to apply the code for carrier dynamics simulation in the considered selectively doped structure, where ionized impurity scattering and electron-electron interaction play a significant role. Carrier dispersion laws, however, were considered to be isotropic, which is a simplification that is rather appropriate for Ge. The purpose of presenting this material is to establish the accuracy of the code by comparison of the results with a variety of well-established experimental characteristics of bulk p-Ge lasers.

The usual approach was to use Debye screening or Conwell-Weisskopf method (see [11, 13]) for ionized impurity scattering. Sometimes a double quantity of scattering centers compared with N_a was used to account for electron-electron interaction. We consider unscreened ionized impurity scattering and scattering on heavy holes separately. Using an unscreened method of Ridley [12] avoids divergence of the probability integral that Debye shielded was previously used to avoid. The difference with previous calculations is that the cross section goes to zero with increasing concentration very quickly after $2*10^{14}$ - $4*10^{14}\,cm^{-3}$, and it gives an optimum concentration of $9*10^{13}\,cm^{-3}$, in close agreement with experiment (see [1]). In contrast, MC simulations with Debye screening predicted optimum concentration higher than $2*10^{14}\,cm^{-3}$ [11]. Fig. A1 shows gain cross section at $100cm^{-1}$ and gain (cross section multiplied by concentration) vs. acceptor concentration without compensation, calculated using the novel methods.

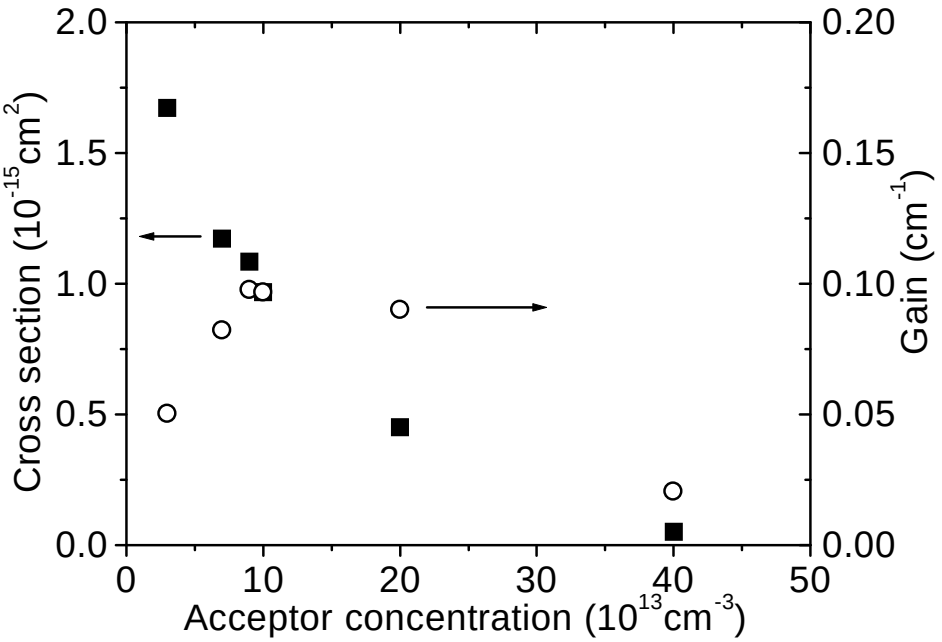

Fig. A1. Gain cross section and optical gain vs. acceptor concentration (zero compensation is assumed).

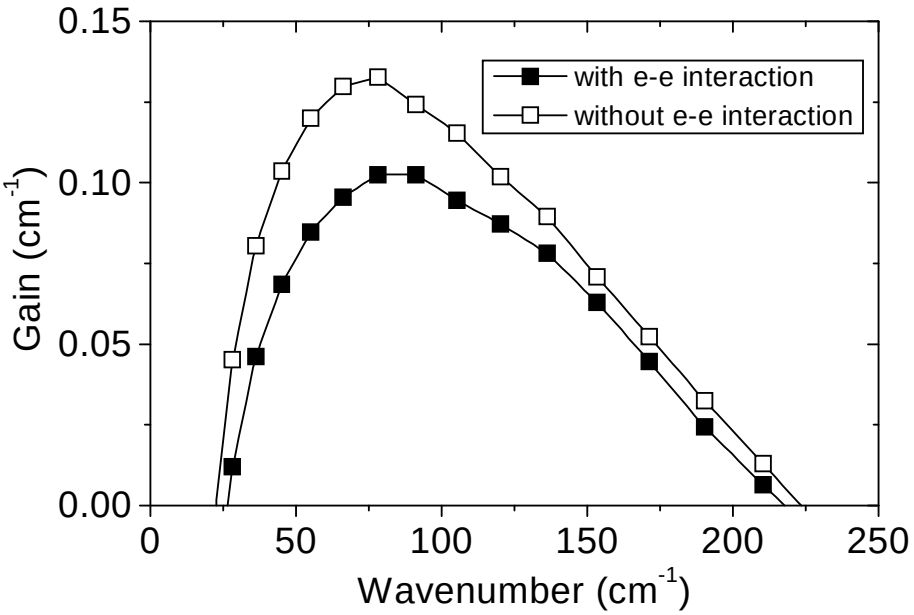

Fig. A2. Comparison of bulk p-Ge crystal gain for $N_a = 9*10^{13}\,cm^{-3}$ with and without electron-electron interaction.

Electron-electron scattering of light holes on heavy holes needs to be considered for accurate gain calculation. Fig. A2 presents gain spectra ($N_a = 9*10^{13}\,cm^{-3}$, compensation is zero) with and without e-e scattering. Electron-electron interaction significantly affects the optical gain of the bulk p-Ge crystal.

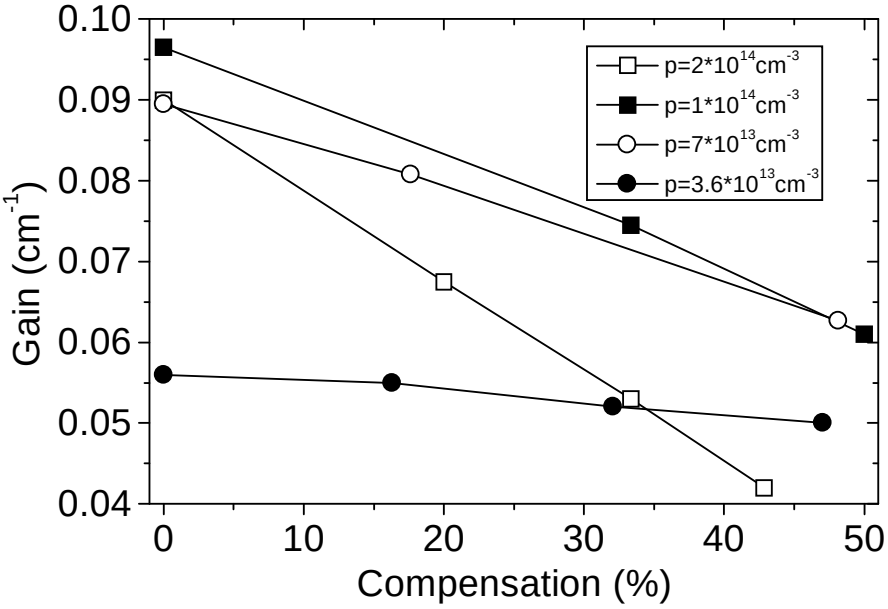

Fig. A3. Bulk p-Ge crystal gain vs. compensation for different hole concentrations with electron-electron interaction included.

Fig. A3 presents new results on the effect of compensation on gain for different net hole concentration. These calculations show a stronger dependence of gain on compensation level than would be obtained using Debye screening model, especially at high concentrations. If non-zero compensation had been assumed in the calculations for Fig. A1, the optimal carrier concentration would have been reduced to levels even closer to the experimentally observed value $\sim 7*10^{13}\,cm^{-3}$ [11, 13].

Fig. A4 presents calculated current density vs. applied electric field to show the saturation due to optical phonon scattering (compare [16]).

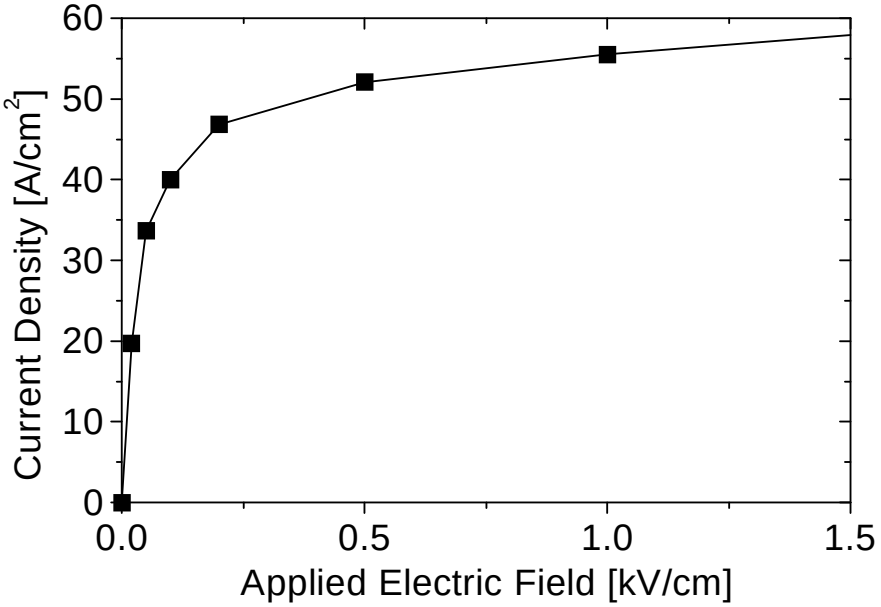

Fig. A4. Current density vs. applied electric field for bulk p-Ge crystal. $N_a = 3.6*10^{13}\,cm^{-3}$, compensation is zero. Electron-electron interaction is not included.

ACKNOWLEDGMENTS

This work was partially supported by subconracts on AFOSR STTR Phase I contract F49620-02-C-0025 and AFOSR STTR Phase II contract F49620-02-C-0027 to Zaubertek and by NSF grant ECS-0070228 to UCF. We thank Dr. Remco Strijbos for initial advice on the Monte Carlo technique.

REFERENCES

1. E. Gornik and A. A. Andronov (eds), "Special issue on far-infrared semiconductor lasers," *Opt. Quantum Electron.* **23** (1991).
2. S. G. Pavlov, Kh. Zhukavin, E. E. Orlova, V. N. Shastin, A. V. Kirsanov, H.-W. Huebers, K. Auien, H. Riemann, "Stimulated emission from donor transitions in silicon," *Phys. Rev. Lett.* **84**, 5220 (2000).
3. B. S. Williams, H. Callebaut, S. Kumar, Q. Hu, J. L. Reno, "3.4 THz quantum cascade laser based on longitudinal-optical-phonon scattering for depopulation," *Appl. Phys. Lett.* **82**, 1015 (2003).
4. R. Kohler, A. Tredicucci, F. Beltram, H. E. Beere, E. H. Linfield, A. G. Davies, D. A. Ritchie, R. C. Iotti and F. Rossi, "Terahertz semiconductor-heterostructure laser", *Nature* **417**, 156 (2002).
5. M. Rochat, L Ajili, H. Willenberg, J. Faist, H. Beere, G. Davies, E. Linfield, and D. Ritchie, "Low-threshold terahertz quantum-cascade lasers", *Appl. Phys. Lett.* **81**, 1381 (2002).
6. C. Jacoboni and L. Reggiani, "The Monte Carlo method for the solution of charge transport in semiconductors with applications of covalent materials," *Rev. Mod. Phys.* **55**, 645 (1983).
7. C. Jacoboni, R. Brunetti and P. Bordone, "Monte Carlo simulation of semiconductor transport," in *Theory of Transport Properties of Semiconductor Nanostructures*, ed. Eckehard Scholl, p. 59 Chapman & Hall, London (1998).
8. G. L. Bir and G. E. Pikus, *Symmetry and strain-induced effects in semiconductors*, (Wiley, NY 1974).
9. P. Lawaetz, "Low-field mobility and galvanomagnetic properties of holes in germanium with phonon scattering", *Phys Rev.* **174**, 867 (1968).
10. J. D. Wiley, "Polar mobility of holes in II-V compounds," *Phys. Rev. B* **4**, 2485 (1970).

11. E.V.Starikov, P.N.Shiktorov, “Numerical simulation of far infrared emission under population inversion of hot sub-bands”, *Optical and Quantum Electronics*, **23**, n.2, 1991, p. S177
12. B. K. Ridley, “Reconciliation of the Conwell-Weisskopf and Brooks-Herring formulae for charged-impurity scattering in semiconductors: Third-body interference”, *J. Phys. C: Solid State Phys.*, **Vol. 10**, 1977
13. V. N. Shastin, “Hot hole inter-sub-band transition p-Ge FIR laser”, *Opt. Quantum Electron.*, **Vol. 23** pp. S111-S131, 1991
14. Yu T. Rebane, “Sum rules for oscillator strength of intersubband and intrasubband transitions of free holes in cubic semiconductors”, *Sov. Phys. Solid State* **25**, 1094 (1983).
15. W. C. Dunlap, Jr., “Diffusion of Impurities in Germanium”, *Phys. Rev*. **94** 1531 (1954).
16. E. W. Nelson, E. S.Flitsiyan, A. V. Muravjov, M. V. Dolguikh, R. E. Peale, S. H. Kleckley, W.G. Vernetson, and V. Z. Tsipin, “Neutron Transmutation Doped Far-infrared p-Ge laser”, in *High-Power Fiber and Semiconductor Lasers*, M. Fallahi and J.V. Maloney, Eds., Proc. SPIE Vol. 4993, pp. 10-19 (2003).